Chemical Science

ROYAL SOCIETY OF CHEMISTRY

EDGE ARTICLE

View Article Online
View Journal | View Issue

Check for updates

Cite this: *Chem. Sci.*, 2024, **15**, 6002

All publication charges for this article have been paid for by the Royal Society of Chemistry

Facile preparation of high-efficiency peroxidase mimics: modulation of the catalytic microenvironment of LDH nanozymes through defect engineering induced by amino acid intercalation†

Dong Han,‡[a] Kui Yang,‡[b] Lanlan Chen,[a] Zhaosheng Zhang,[b] Chen Wang,[a] Hongyuan Yan *[b] and Jia Wen *[a]

Received 20th January 2024
Accepted 15th March 2024

DOI: 10.1039/d4sc00469h

rsc.li/chemical-science

Nanozymes have gained much attention as a replacement for natural enzymes duo to their unique advantages. Two-dimensional layered double hydroxide (LDH) nanomaterials with high physicochemical plasticity are emerging as the main forces for the construction of nanozymes. Unfortunately, high-performance LDH nanozymes are still scarce. Recently, defects in nanomaterials have been verified to play a significant role in modulating the catalytic microenvironment, thereby improving catalytic performances of nanozymes. Therefore, the marriage between defect engineering and LDH nanozymes is expected to spark new possibilities. In this work, twenty kinds of natural amino acids were separately inserted into the interlayer of CoFe-LDH to obtain defect-rich CoFe-LDH nanozymes. The peroxidase (POD)-like activity and catalytic mechanism of the as-prepared LDH nanozymes were systematically studied. The results showed that the intercalation of amino acids can effectively enhance the POD-like activity of LDH nanozymes owing to the increasing oxygen/metal vacancies. And L-cysteine intercalated LDH exhibited the highest catalytic activity ascribed to its thiol group. As a proof of concept, LDH nanozymes with superb POD-like activity were used in biosensing and antibacterial applications. This work suggests that modulating the catalytic microenvironment through defect engineering is an effective way to obtain high-efficiency POD mimics.

Open Access Article. Published on 15 March 2024. Downloaded on 6/15/2025 4:25:20 AM.
This article is licensed under a Creative Commons Attribution-NonCommercial 3.0 Unported Licence.

Introduction

As a new generation of artificial enzymes, nanozymes, which are nanomaterials with enzyme-like activity and which follow enzymatic kinetics, have gained a lot of attention.[1] Two-dimensional layered double hydroxide (LDH) nanomaterials with high physicochemical plasticity are emerging as main forces for the construction of nanozymes.[2,3] LDH is an anionic two-dimensional plate-like nanomaterial consisting of positively charged divalent and trivalent cation layers and anion exchangeable interlayer galleries alternatingly. The flexible composition of LDH enables the metal cations and defect sites in the LDH layer to be tailored to mimic the properties of natural enzymes.[4] Therefore, LDH nanozymes are considered to have excellent potential for biocatalysis and biomedicine.

To meet the high requirements of practical applications, the performances of nanozymes are improved by accurately adjusting their components, sizes and so on.[5] However, the activity of most nanozymes is relatively low in comparison with that of natural enzymes. How the development of effective strategies to achieve the preparation of high-performance nanozyme has always been a key issue in the field of nanozyme research. As for LDH nanozymes, various strategies have been developed to enhance their catalytic activities, such as multi-metal coordination, intercalation of functional molecules, exfoliation of the layer and combination of other materials. Unfortunately, LDH nanozymes with high catalytic activity are still scarce.

The catalytic microenvironment is very important for nanozymes to exert catalytic activity, so it is expected that highly active nanozymes can be obtained by the directional modification of the catalytic microenvironment. For example, Yan's group reported that the introduction of histidine residues onto

[a]*State Key Laboratory of New Pharmaceutical Preparations and Excipients, Key Laboratory of Medicinal Chemistry and Molecular Diagnosis of the Ministry of Education, College of Pharmaceutical Science, Hebei University, Baoding 071002, P. R. China. E-mail: wenjiahbu@163.com*

[b]*State Key Laboratory of New Pharmaceutical Preparations and Excipients, Key Laboratory of Medicinal Chemistry and Molecular Diagnosis of Ministry of Education, College of Chemistry and Materials Science, Hebei University, Baoding 071002, P. R. China. E-mail: yanhy@hbu.edu.cn*

† Electronic supplementary information (ESI) available. See DOI: https://doi.org/10.1039/d4sc00469h

‡ These authors contributed equally to this work.

© 2024 The Author(s). Published by the Royal Society of Chemistry

Open Access Article. Published on 15 March 2024. Downloaded on 6/15/2025 4:25:20 AM. This article is licensed under a Creative Commons Attribution-NonCommercial 3.0 Unported Licence.

the Fe_3O_4 nanoparticle surface to mimic the enzymatic microenvironment of natural peroxidase (POD) enzymes can enhance the catalytic efficiency of Fe_3O_4 nanozyme effectively.[6] Qu's group constructed a highly active single-atom nanozyme by modifying sulfonic acid groups on the surface of Fe–N_4 centers.[7] The oxidized sulfur functionalities could assist in substrate orientation and facilitate the desorption of H_2O, and thereby improve the specific activity of nanozymes. Specifically, the optimization of the catalytic microenvironment of LDH nanozymes can be achieved by molecular intercalation, which can generate more oxygen vacancies (V_O) or metal vacancies (V_M), a kind of point defect. Amino acids are the basic units of peptides and proteins, and are closely related to many life activities. Many amino acid residues are also catalytically active sites for natural enzymes, which can promote the binding of enzymes to substrates. Thereby, defect engineering induced by amino acids is expected to be an effective strategy to enhance the catalytic activities of LDH nanozymes.

Herein, in this work, CoFe-LDH with good POD-like activity was selected as the research object. As shown in Scheme 1, twenty kinds of natural amino acids were separately inserted into the interlayer of CoFe-LDH by a facile coprecipitation process along with an ultrasonic-assisted ion exchange reaction, to increase the V_O/V_M in the structure of CoFe-LDH, so as to regulate the catalytic microenvironment of CoFe-LDH and thereby improve its catalytic activity. The results indicated that the POD-like activity of L-cysteine (L-Cys)-intercalated CoFe-LDH (L-C-LDH) was the strongest in comparison with that of other amino acid-intercalated CoFe-LDH (L-AA-LDH) and pristine CoFe-LDH. It is well-known that L-Cys is unique amongst the twenty natural amino acids as it contains a thiol group (–SH), which is a versatile functional group with strong binding affinity and reactivity. It was speculated that the –SH of L-Cys was crucial for the enhancement of the catalytic activity of LDH nanozyme. To confirm this conjecture, different analogues of L-Cys were further prepared and intercalated into CoFe-LDH, respectively. And their POD-like activity and catalytic mechanism were systematically studied. Finally, LDH nanozymes with superb POD-like activity were used in biosensing and antibacterial applications.

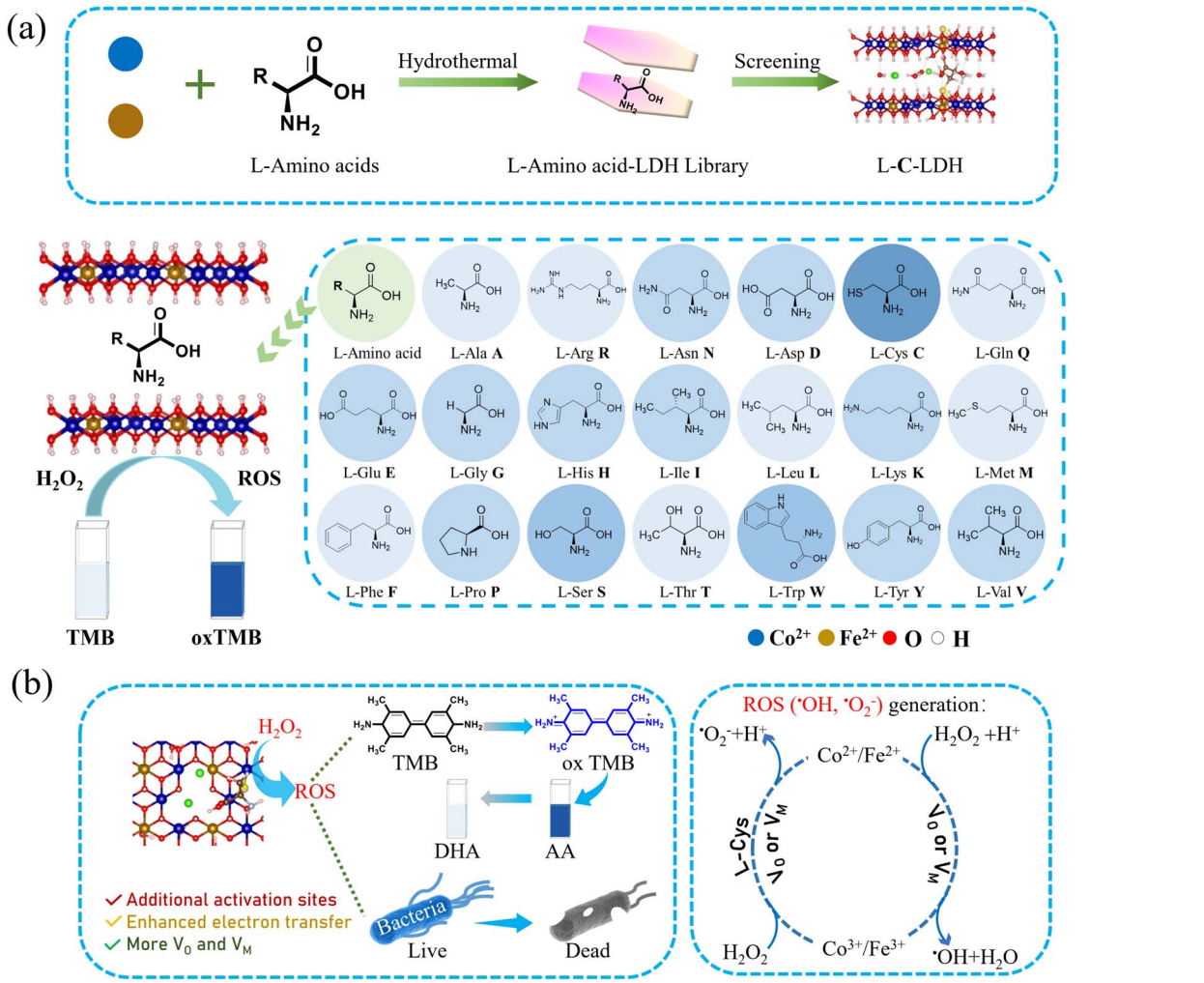

Scheme 1 Schematic diagram of (a) the synthesis and screening of L-AA-LDH nanozymes with superior POD-like activity and (b) their catalysis mechanism and applications.

Open Access Article. Published on 15 March 2024. Downloaded on 6/15/2025 4:25:20 AM. This article is licensed under a Creative Commons Attribution-NonCommercial 3.0 Unported Licence.

Results and discussion

Synthesis and characterization of LDH nanozymes

CoFe-LDH nanozyme and twenty kinds of L-AA-LDH nanozymes were synthesized, respectively. The morphology and structure of the as-prepared LDH nanozymes were characterized by transmission electron microscopy (TEM). As shown in Fig. S1a and b,† a layered structure with a typical regular hexagonal morphology of CoFe-LDH nanozyme can be observed along with a nanosheet size of about 100 nm and a thickness of about 1.8 nm. In comparison with CoFe-LDH nanozyme, L-C-LDH nanozyme displayed a small layer size, which was around 50 nm (Fig. 1a). A loose and small-size structure could provide abundant active functional groups and large specific surface area, which might be beneficial for the catalytic performance of the catalyst.[8] And the thickness of L-C-LDH nanozyme was about 1.8–1.9 nm (Fig. 1b). Elemental distribution mapping showed the presence of C, N, O, Co, Fe and S and their homogeneous distribution in L-C-LDH nanozyme (Fig. 1c). The crystal structures of CoFe-LDH nanozyme and L-C-LDH nanozyme were tested by X-ray powder diffraction (XRD) (Fig. 1d). In the pattern of CoFe-LDH nanozyme, the obvious peaks at 2θ of 11.52°, 22.93°, 34.21° and 59.29° were ascribed to the (003), (006), (009) and (110) planes of a typical CoFe-LDH (JCPDS No. 50-0235).[9,10] The clear diffraction peaks indicated the high crystallinity of CoFe-LDH nanozyme. And L-C-LDH nanozyme retained the original phase of CoFe-LDH. In particular, the (003) peak of L-C-LDH nanozyme (11.06°) was of a smaller angle than that of CoFe-LDH nanozyme. Based on the calculation by Bragg's law,[11] the basal spacing (d_{003}) of CoFe-LDH nanozyme was 0.767 nm, while that of L-C-LDH nanozyme was enlarged to 0.799 nm. The increased interlayer spacing confirmed the successful insertion of Cys.[12] Fig. S1c and S8a† show Fourier transform infrared (FT-IR) spectra, which indicated the stretching vibration of O–H,[13] the asymmetric and symmetric stretching vibrations of –COO[14] and the lattice vibration of M–O or O–M–O (M = Co, Fe)[15] in LDH nanozymes. In addition, according to Table S1,† the distribution proportion of the element S in L-C-LDH nanozyme was 3.4% obtained by inductively coupled plasma optical emission spectrometry (ICP-OES). The zeta potentials of CoFe-LDH nanozyme and L-C-LDH nanozyme in deionized (DI) water were +14.78 mV and −22.09 mV, respectively (Fig. S2 and S3†), further indicating the successful insertion of Cys. Thermogravimetric-differential thermal analysis (TG-DTA) results also confirmed the insertion of Cys (Fig. S4†).

To investigate the surface elemental composition and valence states of the as-prepared LDH nanozymes, X-ray photoelectron spectroscopy (XPS) was conducted. Fig. S1d† showed peaks from the XPS survey spectrum of CoFe-LDH nanozyme, which were mainly attributed to Co 2p, Fe 2p, C 1s, O 1s and Cl 2p regions. In

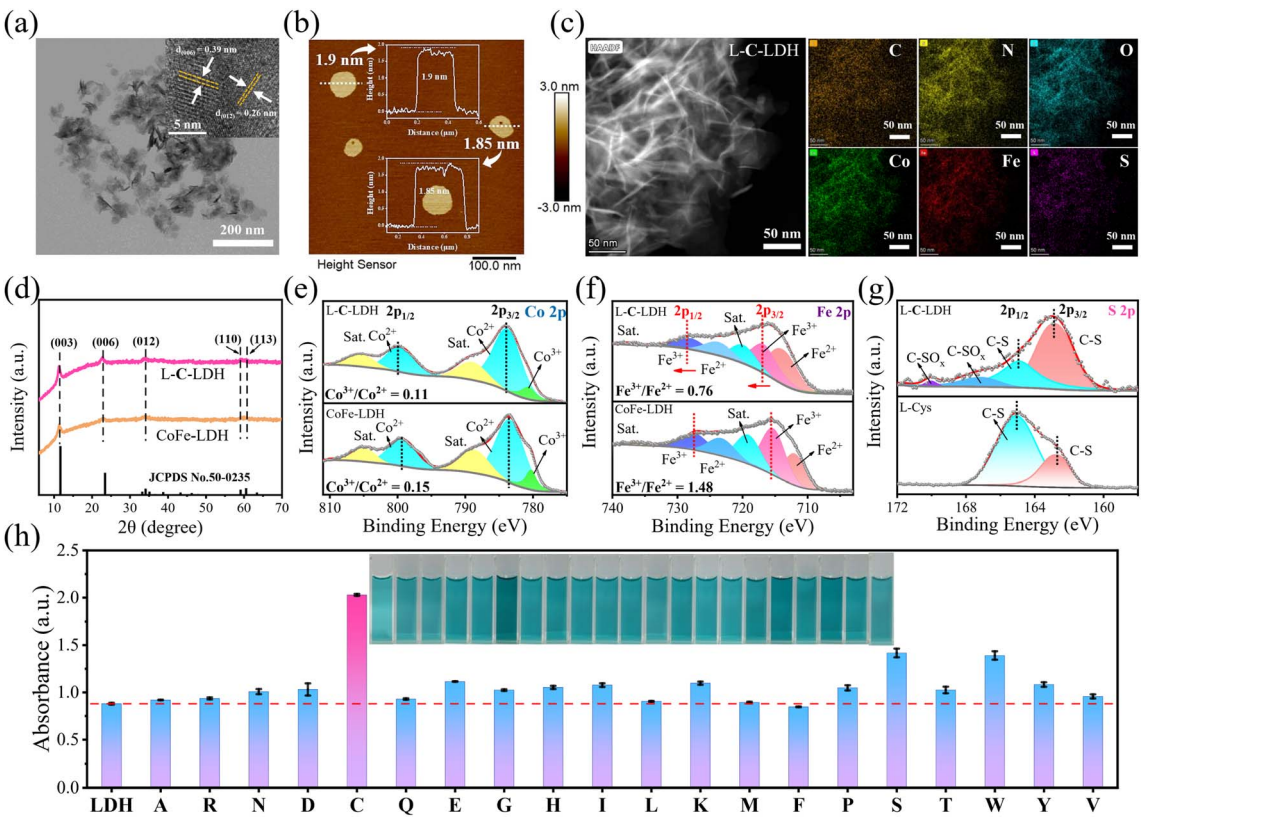

Fig. 1 Characterization of LDH nanozymes. (a) TEM and HRTEM (inset) images, (b) AFM image, and (c) TEM elemental mapping of L-C-LDH nanozyme. (d) XRD patterns of CoFe-LDH nanozyme and L-C-LDH nanozyme. High-resolution XPS spectra of (e) Co 2p, (f) Fe 2p and (g) S 2p regions of CoFe-LDH nanozyme and L-C-LDH nanozyme. (h) The comparison of the absorbance at 652 nm of CoFe-LDH nanozyme and different L-AA-LDH nanozymes. Insets show the corresponding color changes of TMB in different systems.

© 2024 The Author(s). Published by the Royal Society of Chemistry

Open Access Article. Published on 15 March 2024. Downloaded on 6/15/2025 4:25:20 AM. This article is licensed under a Creative Commons Attribution-NonCommercial 3.0 Unported Licence.

the XPS survey spectrum of L-**C**-LDH nanozyme (Fig. S9b†), new N 1s and S 2p peaks could be found. This further indicated that Cys was intercalated into CoFe-LDH. As shown in Fig. 1e, the Co 2p XPS spectrum of CoFe-LDH nanozyme showed two peaks corresponding to Co^{2+} and Co^{3+} (783.48 and 799.28 eV for Co^{2+} and 780.20 eV for Co^{3+}), while the other two peaks at 788.66 eV and 804.77 eV were doublet satellite (Sat.) peaks of Co $2p_{3/2}$ and Co $2p_{1/2}$, respectively. As for L-**C**-LDH nanozyme, the pair of peaks for Co^{2+} shifted towards low binding energy (shifted by about 0.26 eV for Co $2p_{3/2}$ and 0.25 eV for Co $2p_{1/2}$), indicating that the electron density of metal layers in CoFe-LDH decreased after the intercalation of Cys.[16] Meanwhile, the content of Co^{2+} in L-**C**-LDH nanozyme was slightly increased compared with that in CoFe-LDH nanozyme. Analogously, the pair of peaks for Fe^{3+} in L-**C**-LDH nanozyme shifted towards low binding energy (shifted by about 1.44 eV for Fe $2p_{3/2}$ and 0.60 eV for Fe $2p_{1/2}$) compared with that of CoFe-LDH nanozyme (Fig. 1f).[11,17,18] In addition, the content of Fe^{2+} in L-**C**-LDH nanozyme was significantly increased compared with that in CoFe-LDH nanozyme. And the ratio change of Co^{3+}/Co^{2+} was consistent with that of Fe^{3+}/Fe^{2+} in the nanozyme. This may be ascribed to the V_O formed by the intercalation of amino acids. The S 2p XPS spectrum of L-**C**-LDH nanozyme showed two distinct peaks centered at 162.80 eV and 164.91 eV, corresponding to C–S $2p_{3/2}$ and C–S $2p_{1/2}$, respectively, which were lower than that of L-Cys (Fig. 1g).[19] And the two peaks at 167.12 eV and 170.04 eV were ascribed to C–SO_x, which may be produced from the partial oxidation of C–SH in an alkaline solution.[20,21] The characterization studies of other L-AA-LDH nanozymes are illustrated in the ESI (Fig. S5–S24 and Table S2†).

Screening the catalytic activity of LDH nanozymes

To demonstrate the catalytic activities of CoFe-LDH nanozyme and L-AA-LDH nanozymes as POD-like mimics, the catalytic oxidation of 3,3,5,5-tetramethylbenzidine (TMB) by LDH nanozymes was determined. As illustrated in Fig. 1h and S25,† the CoFe-LDH/TMB/H_2O_2 system exhibited an enhanced absorbance at 652 nm in comparison with pure H_2O_2/TMB and the CoFe-LDH/TMB system. And its solution was blue. These results demonstrated that CoFe-LDH nanozyme exhibited POD-like activity. In addition, various L-AA-LDH/TMB/H_2O_2 systems showed different absorbance intensities at 652 nm, all of which were stronger than that of the CoFe-LDH/TMB/H_2O_2 system, indicating that the intercalation of amino acids can enhance the POD-like activity of CoFe-LDH nanozyme. Notably, the L-**C**-LDH/TMB/H_2O_2 system exhibited the highest absorption peak intensity at 652 nm, which was about 2.31 times that of the CoFe-LDH/TMB/H_2O_2 system. It was speculated that the active reducing –SH of L-Cys played a critical role.[8]

In order to explore the reason for the enhancement of the POD-like activity of L-**C**-LDH nanozyme, different Cys derivative-intercalated CoFe-LDH (**C**-LDH) nanozymes were prepared for comparison. The characterization studies of a series of **C**-LDH nanozymes are illustrated in the ESI (Fig. S26–S35 and Table S3†). As shown in Fig. 2a, different Cys derivatives (methionine (L-Met), cystine (Cys–Cys), *N*-acetyl-L-cysteine (Acet-L-Cys), L-cysteine methyl ester (Me-L-Cys), and L-cysteine ethyl ester (Et-L-Cys)) were prepared. And the corresponding Cys derivative-intercalated CoFe-LDH nanozymes were named in turn as L-**M**-LDH, **C**-**C**-LDH, Acet-L-**C**-LDH, Me-L-**C**-LDH and Et-L-**C**-LDH. As illustrated in Fig. 2b and c and S36,† compared to the CoFe-LDH/TMB/H_2O_2 system, the absorbance intensities of different **C**-LDH/TMB/H_2O_2 systems were increased to different degrees, the order of which was Me-L-**C**-LDH > L-**C**-LDH > L-**C**-LDH (HCl) > Et-L-**C**-LDH > **C**-**C**-LDH > D-**C**-LDH > Acet-L-**C**-LDH > L-**M**-LDH. These results may be because the lack of electron-rich regions of –SH groups in L-Met and Cys–Cys lead to the reduction of catalytic activity of L-**M**-LDH and **C**-**C**-LDH compared with that of L-**C**-LDH. The amino group, which is an electron-rich region, in Acet-L-**C**-LDH was replaced by an electron-deficient acetyl group, resulting in a decrease in its catalytic activity. This also suggested that –SH and $–NH_2$ groups (containing lone pair electrons and electron-rich regions) played a catalytic role in the reaction (electron-donating). The –COOH groups of Me-L-Cys and Et-L-Cys were replaced by methyl ester and ethyl ester groups, which increased the steric hindrance during intercalation. The steric hindrance of Et-L-Cys was higher due to its larger molecular weight than methyl ester, resulting in a decrease in its catalytic activity.

The optimum catalytic conditions of LDH nanozymes were further screened, and the effects of pH values and temperature on the POD-like activity of LDH nanozymes were investigated (Fig. 2d and e). The results showed that the POD-like activity of LDH nanozymes was affected by pH and temperature. The catalytic activity of LDH nanozymes was the highest at pH 3.0 and 50 °C, respectively. In addition, the absorbance at 652 nm of various LDH nanozymes also increased over time (Fig. 2f), and 10 min was selected as the incubation time.

In order to further investigate the catalytic activities of LDH nanozymes as POD mimics, the POD-like activity of LDH nanozymes was detected by changing the concentration of TMB or H_2O_2 to obtain kinetic parameters, namely the Michaelis constant (K_m) and the maximum initial reaction rate (V_{max}), which could be calculated *via* fitting the Michaelis–Menten curve.[22] CoFe-LDH nanozyme, L-**C**-LDH nanozyme and Me-L-**C**-LDH nanozyme were selected for comparison. The steady-state kinetic curve and the corresponding double-reciprocal plot of LDH nanozymes with varied concentrations of TMB and H_2O_2 at 37 °C are illustrated in Fig. 3 and S37–S39.† The results indicated that all LDH nanozymes exhibited lower K_m and higher V_{max} than that of natural horseradish peroxidase (HRP). And Me-L-**C**-LDH nanozyme exhibited the lowest K_m and highest V_{max}. In addition, the results obtained at 25 °C showed a consistent trend (Fig. S40–S42†). The comparison of the K_m and V_{max} between this work and reported nanozymes is illustrated in Table S4.† Moreover, LDH nanozymes could maintain their catalytic activities after repeated use (Fig. S43–S46†).

Proposed catalysis mechanism of LDH nanozymes as POD mimics

To reveal the catalysis mechanism of LDH nanozymes, the main reactive oxygen species (ROS) were identified through quenching experiments and electron paramagnetic resonance (EPR)

Open Access Article. Published on 15 March 2024. Downloaded on 6/15/2025 4:25:20 AM.
This article is licensed under a Creative Commons Attribution-NonCommercial 3.0 Unported Licence.

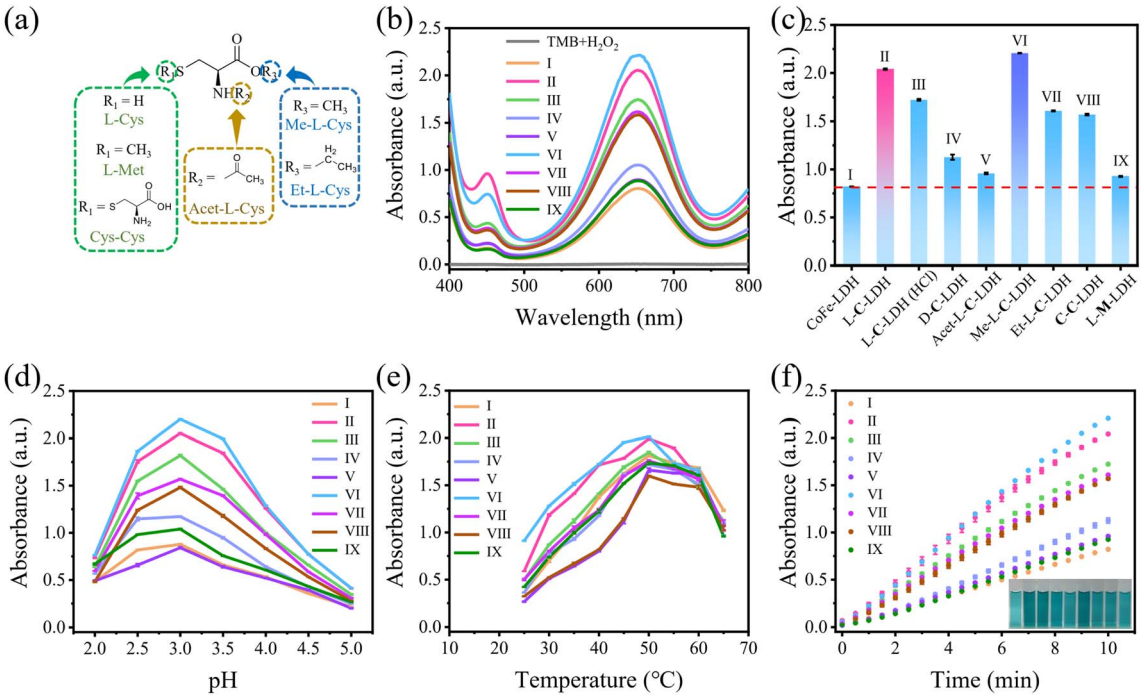

Fig. 2 (a) Structures of L-Cys derivatives. (b) UV-vis absorption spectra of different reaction systems and (c) the corresponding absorbance at 652 nm. (d) pH, (e) temperature and (f) time-dependent POD-like activity of different reaction systems. Insets show the color changes of different systems (I: CoFe-LDH/TMB/H_2O_2, II: L-**C**-LDH/TMB/H_2O_2, III: L-**C**-LDH (HCl)/TMB/H_2O_2, IV: D-**C**-LDH/TMB/H_2O_2, V: Acet-L-**C**-LDH/TMB/H_2O_2, VI: Me-L-**C**-LDH/TMB/H_2O_2, VII: Et-L-**C**-LDH/TMB/H_2O_2, VIII: **C**-**C**-LDH/TMB/H_2O_2, and IX: L-**M**-LDH/TMB/H_2O_2).

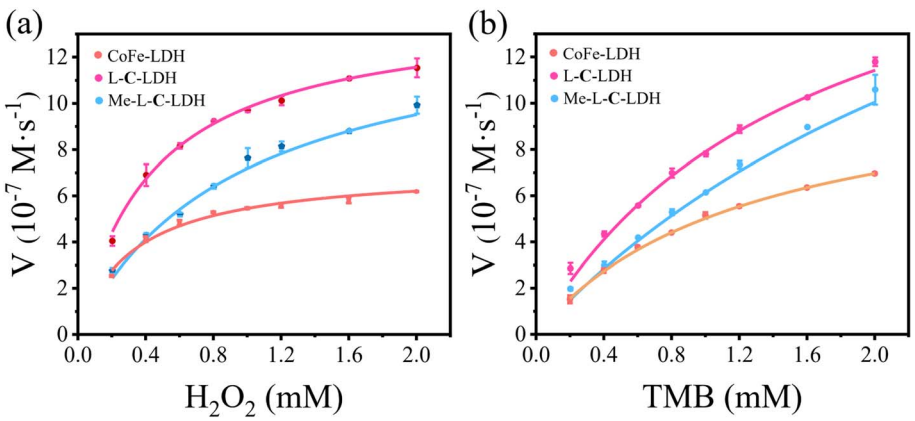

Fig. 3 Steady-state kinetic curve of CoFe-LDH nanozyme, L-**C**-LDH nanozyme and Me-L-**C**-LDH nanozyme with varied concentrations of (a) H_2O_2 and (b) TMB, respectively. The reaction rate *versus* H_2O_2 concentration at a fixed concentration of TMB (1.50 mM). The reaction rate *versus* TMB concentration at a fixed concentration of H_2O_2 (1.50 mM).

analysis. ·OH and $\cdot O_2^-$ are generally considered to be the main ROS formed in catalytic wet oxidation systems. Thus, thiourea (TH) and *p*-benzoquinone (*p*-BQ) were used as the scavengers for ·OH and $\cdot O_2^-$, respectively. As shown in Fig. 4a–c, the addition of TH and *p*-BQ significantly inhibited the absorption intensity at 652 nm of CoFe-LDH/TMB/H_2O_2, L-**C**-LDH/TMB/H_2O_2 and Me-L-**C**-LDH/TMB/H_2O_2 systems, while O_2 had no significant effect on the systems, indicating that ·OH and $\cdot O_2^-$ were the main ROS generated in the reaction system.[23] To gain further evidence, 5,5-dimethyl-1-pyrroline-1-oxide (DMPO) was used as a free radical trapping agent for ·OH and $\cdot O_2^-$. As shown in Fig. 4e and f, in comparison with pure H_2O_2, obvious signals of DMPO–·OH and DMPO–$\cdot O_2^-$ could be observed in CoFe-LDH/H_2O_2, L-**C**-LDH/H_2O_2 and Me-L-**C**-LDH/H_2O_2 systems, indicating the generation of ·OH and $\cdot O_2^-$. Another trapping agent 5-*tert*-butoxycarbonyl 5-methyl-1-pyrroline *N*-oxide (BMPO) was used to repeat the experiments, and consistent results were obtained (Fig. S47†). In addition, at around $g = 2.004$, all of LDH nanozymes showed strong symmetric EPR signals (Fig. 4d), which can be attributed to paramagnetic V_O.[24] And Me-L-**C**-LDH nanozyme and L-**C**-LDH nanozyme had stronger signal peaks than that of CoFe-LDH nanozyme, which

© 2024 The Author(s). Published by the Royal Society of Chemistry

Open Access Article. Published on 15 March 2024. Downloaded on 6/15/2025 4:25:20 AM. This article is licensed under a Creative Commons Attribution-NonCommercial 3.0 Unported Licence.

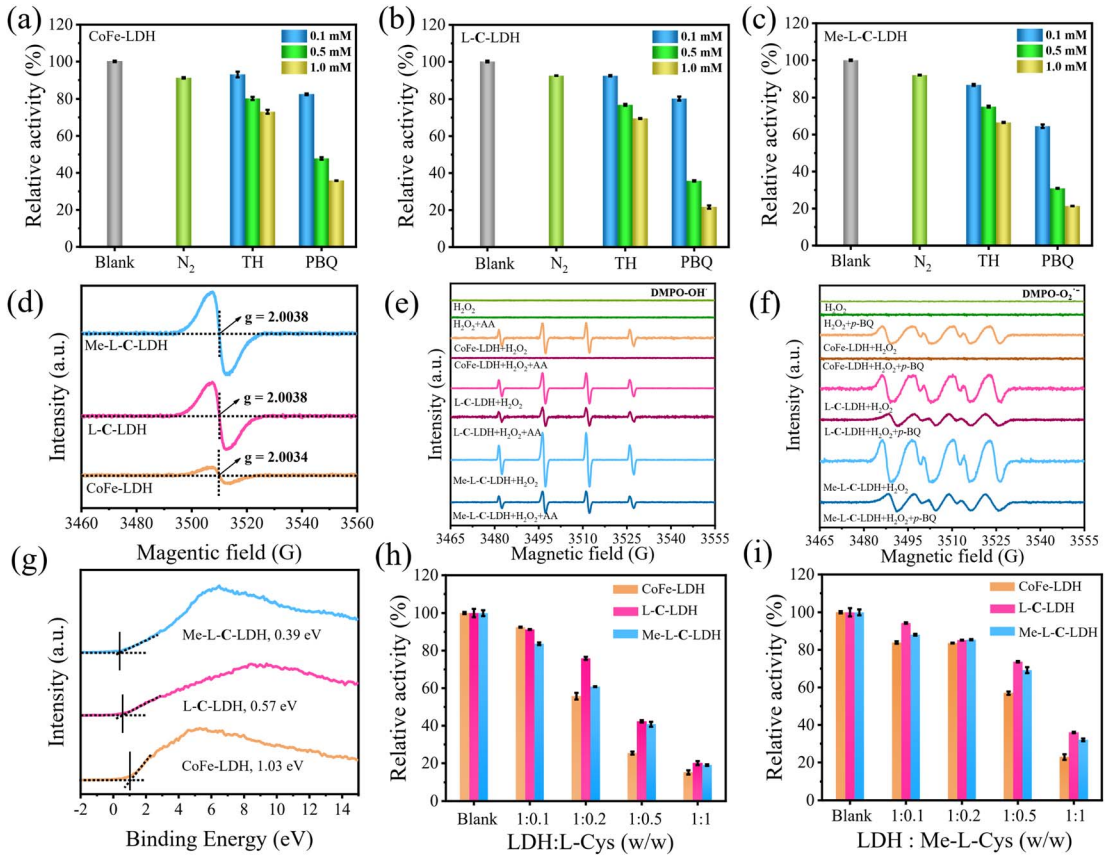

Fig. 4 The absorbance at 652 nm of (a) CoFe-LDH/TMB/H_2O_2 system, (b) L-**C**-LDH/TMB/H_2O_2 system and (c) Me-L-**C**-LDH/TMB/H_2O_2 system in the presence of different concentrations of ROS scavengers. (d) EPR spectra of CoFe-LDH nanozyme, L-**C**-LDH nanozyme and Me-L-**C**-LDH nanozyme. EPR signals of the (e) DMPO–·OH adduct and (f) DMPO–$\cdot O_2^-$ adduct in CoFe-LDH/H_2O_2, L-**C**-LDH/H_2O_2 and Me-L-**C**-LDH/H_2O_2 systems. (g) Valence band structure of CoFe-LDH nanozyme, L-**C**-LDH nanozyme and Me-L-**C**-LDH nanozyme. Relative activity of CoFe-LDH/TMB/H_2O_2, L-**C**-LDH/TMB/H_2O_2 and Me-L-**C**-LDH/TMB/H_2O_2 systems with different weights of (h) L-Cys and (i) Me-L-Cys, respectively.

indicated that Me-L-**C**-LDH nanozyme and L-**C**-LDH nanozyme had more abundant V_O,[25,26] which would greatly affect their electronic properties and catalytic properties.[27] Furthermore, the valence band obtained from XPS spectra of LDH nanozymes was also studied. As shown in Fig. 4g, the maximum valence band energy of CoFe-LDH nanozyme was 1.03 eV, while the maximum valence band energy of L-**C**-LDH nanozyme and Me-L-**C**-LDH nanozyme was about 0.57 eV and 0.39 eV, respectively, both of which blue shifted to the vacuum level. These results demonstrated that Me-L-**C**-LDH nanozyme and L-**C**-LDH nanozyme had a lower electron transfer barrier due to the intercalation of Me-L-Cys and L-Cys, which was more favorable to electron transfer.[28] As shown in Fig. 4h and i, after the addition of different mass ratios of L-Cys/Me-L-Cys into the CoFe-LDH/TMB/H_2O_2, L-**C**-LDH/TMB/H_2O_2 and Me-L-**C**-LDH/TMB/H_2O_2 systems, the absorbance at 652 nm decreased to different degrees. This demonstrated that free L-Cys/Me-L-Cys may inhibit the catalytic activity of LDH nanozymes. This was mainly because both L-Cys and Me-L-Cys contained active reducing –SH groups, which may reduce blue oxTMB to colorless TMB, resulting in reduced catalytic activity. These results further proved that only intercalated amino acids but not free amino acids can enhance the catalytic activity of LDH nanozymes.

To further investigate the changes in various types of oxygen and the presence of V_O in LDH nanozymes, the XPS spectra of O 1s were further obtained in addition to EPR tests. The four fitting peaks in the XPS spectrum of CoFe-LDH nanozyme correspond to metal–oxygen (M–O, M = Co, Fe) in the lattice, oxygen atoms in the hydroxyl group (M–OH), V_O and surface-bound water molecules, the binding energy of which was 529.31 eV, 530.99 eV, 532.36 eV and 533.96 eV, respectively (Fig. 5a).[4,18,27,29] And the percentage of V_O was 22.50%. The fitting characteristic peaks of L-**C**-LDH nanozyme and Me-L-**C**-LDH nanozyme were consistent with that of CoFe-LDH nanozyme (Fig. 5b and c). In particular, the percentage of V_O in L-**C**-LDH nanozyme and Me-L-**C**-LDH nanozyme was 24.92% and 44.12%, separately. It was further proved that the POD-like activities of Me-L-**C**-LDH nanozyme and L-**C**-LDH nanozyme were stronger than that of CoFe-LDH nanozyme due to the increase in the content of V_O, which was consistent with the results of the EPR test. In order to further explore the effects of amino acid intercalation on the coordination environment and chemical state of CoFe-LDH, X-ray absorption fine structure (XAFS) was applied to study the structure of LDH nanozymes. And the valence states of Co and Fe were characterized by X-ray absorption near edge structure (XANES) spectroscopy. As shown

Open Access Article. Published on 15 March 2024. Downloaded on 6/15/2025 4:25:20 AM.
This article is licensed under a Creative Commons Attribution-NonCommercial 3.0 Unported Licence.

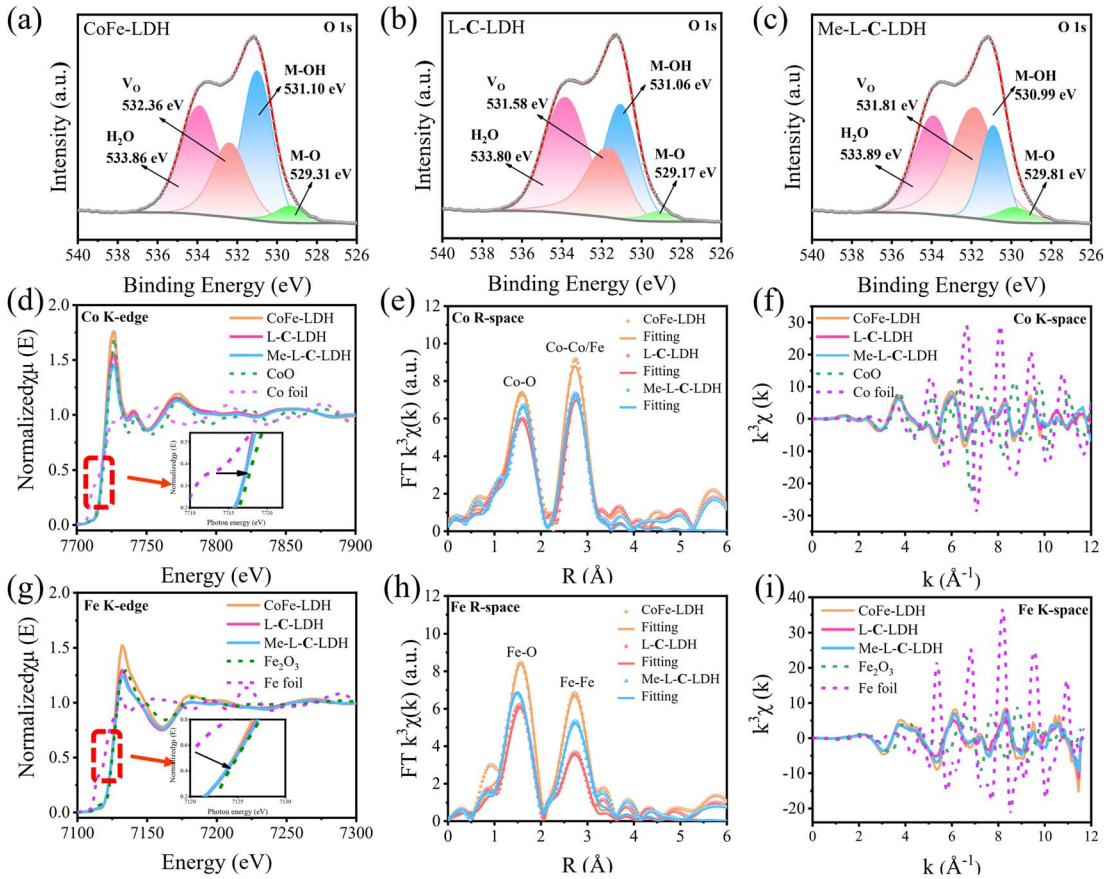

Fig. 5 High-resolution XPS spectra of O 1s for (a) CoFe-LDH nanozyme, (b) L-C-LDH nanozyme and (c) Me-L-C-LDH nanozyme. (d) Co K-edge and (g) Fe K-edge XANES spectra of CoFe-LDH nanozyme, L-C-LDH nanozyme and Me-L-C-LDH nanozyme in comparison with those of CoO, Co foil, Fe_2O_3 and Fe foil. (e) Co K-edge and (h) Fe K-edge Fourier transform spectra with fitting results of CoFe-LDH nanozyme, L-C-LDH nanozyme and Me-L-C-LDH nanozyme. (f) Co K-edge and (i) Fe K-edge extended XAFS $k^3\chi(k)$ oscillation functions for CoFe-LDH nanozyme, L-C-LDH nanozyme and Me-L-C-LDH nanozyme.

in Fig. 5d, Co foil and CoO were selected as reference. The characteristic peaks in XANES spectra of CoFe-LDH nanozyme, L-C-LDH nanozyme and Me-L-C-LDH nanozyme were higher than that of Co foil but lower than that of CoO, indicating that the oxidation state of Co in LDH nanozymes was increased.[30] Similarly, the absorption edges of the Fe K-edge XANES spectra of CoFe-LDH nanozyme, L-C-LDH nanozyme and Me-L-C-LDH nanozyme were between those of Fe foil and Fe_2O_3 (Fig. 5g), and were very close to those of Fe_2O_3, indicating that Fe carried a positive charge in LDH nanozymes.[31,32] The corresponding Co K-edge $k^3\chi(k)$ oscillation curves (Fig. 5f) of L-C-LDH nanozyme and Me-L-C-LDH nanozyme showed a reduction in the oscillation amplitude compared to that of CoFe-LDH nanozyme, and the corresponding Fe K-edge $k^3\chi(k)$ oscillation curves of LDH nanozymes (Fig. 5i) also showed consistent results, revealing a structural change in the coordination environment of the Co atoms and Fe atoms. Moreover, the first derivative obtained by Fourier transformed extended X-ray absorption fine structure (FT-EXAFS) fitting revealed the oxidation states of Co and Fe (Tables S5 and S6†). In particular, FT-EXAFS spectra also provided detailed coordination number (CN) information for the first layer Co–O (at about 2.07 Å) and second layer Co–Co/Fe (at about 3.14 Å) of LDH nanozymes.[30] As illustrated in Fig. 5e and Table S5,† the CN of Co–O and Co–Co/Fe in L-C-LDH nanozyme and Me-L-C-LDH nanozyme was lower than that in CoFe-LDH nanozyme, revealing the presence of more V_O and V_M (cobalt and iron vacancies (V_{Co} and V_{Fe})). Similarly, the CN of Fe–O and Fe–Fe in L-C-LDH nanozyme and Me-L-C-LDH nanozyme was lower than that in CoFe-LDH nanozyme, again verifying the presence of more V_O and V_{Co}/V_{Fe} (Fig. 5h and Table S6†). Furthermore, in comparison with CoFe-LDH nanozyme, L-C-LDH nanozyme and Me-L-C-LDH nanozyme had a lower Debye–Waller factor, which also revealed the increase in the disorder degree, demonstrating the presence of the structure distortion and dangling band on the surface Co atom in L-AA-LDH nanozymes.[30] From the above analysis, L-AA-LDH nanozymes had a lower CN, increased structure distortion and dangling bands on the surface, which could serve as the catalytically active sites to enhance their POD-like activities.

Furthermore, density functional theory (DFT) calculations were used to investigate the catalytic mechanism of LDH nanozymes deeply. Based on the results of PXRD, XPS, EPR and XAFS, the models of CoFe-LDH nanozyme, L-C-LDH nanozyme and Me-L-C-LDH nanozyme were constructed, and the free energy graphs of POD reactions of different nanozymes were calculated respectively. The optimal adsorption site (Co or Fe)

© 2024 The Author(s). Published by the Royal Society of Chemistry

Open Access Article. Published on 15 March 2024. Downloaded on 6/15/2025 4:25:20 AM. This article is licensed under a Creative Commons Attribution-NonCommercial 3.0 Unported Licence.

can be determined by using the Gibbs free energy difference (ΔG) of the reaction with each intermediate.[33] The energy diagrams of the homolytic path and heterolytic path of H_2O_2 on different metal atoms are illustrated in Fig. 6 and S48,† separately. The results indicated that after activation, the reaction intermediate (2*OH) adsorbed by LDH nanozymes through the homolytic path had more negative Gibbs free energy than the *O and *H_2O produced by the heterolytic path, indicating that the adsorption capacity of 2*OH was stronger, and thereby the homolytic path was more likely to occur.[34]

The homolytic path can be categorized into Fe sites-prior (Fig. 6a) and Co sites-prior (Fig. 6b) according to the priority of the reaction site. As for CoFe-LDH nanozyme, either Fe sites-prior or Co sites-prior, it had the weakest adsorption strength to the H_2O molecules generated by the reaction during the second hydrogenation and positive ΔG, which made it harder for the reaction to occur compared to L-C-LDH nanozyme and Me-L-C-LDH nanozyme. These results indicated that the catalytic activity of L-C-LDH nanozyme and Me-L-C-LDH nanozyme was higher than that of CoFe-LDH nanozyme. As for Fe sites-prior, L-C-LDH nanozyme exhibited higher catalytic activity than Me-L-C-LDH nanozyme. This was because that when Fe atoms acted as the *OH adsorption site for the first hydrogenation reaction, the Fe in Me-L-C-LDH nanozyme had a weaker adsorption strength for the H_2O molecules generated by the hydrogenation than L-C-LDH nanozyme, which resulted in a higher Gibbs free energy, thus making it more difficult for the reaction to occur (Fig. 6a).[35] As for Co sites-prior, Me-L-C-LDH nanozyme exhibited higher catalytic activity than L-C-LDH nanozyme. This was because when Fe atoms were used as adsorption sites in the second hydrogenation reaction, L-C-LDH nanozyme adsorbed weakly to the H_2O molecules generated by the second hydrogenation, resulting in a higher Gibbs free energy, thereby making it harder for the reaction to occur (Fig. 6b). The above results indicated that L-C-LDH nanozyme and Me-L-C-LDH nanozyme were more conducive to the reaction than CoFe-LDH nanozyme, verifying that amino acid intercalated LDH nanozymes had stronger catalytic activity. This was mainly because the –SH group of L-Cys and Me-L-Cys acted as the electron donor to coordinate with Co and Fe sites, which enhanced the electron transfer between LDH nanozymes and reaction intermediates. Meanwhile, the intercalation of amino acids introduced more V_O and V_M, thereby resulting in more active sites and decreasing adsorption energy between active sites and intermediates.

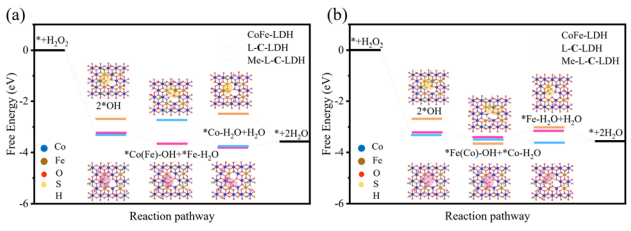

Fig. 6 DFT studies on the POD-like activity of LDH nanozymes. The activation process of H_2O_2 by the homolytic path at (a) Fe sites-prior and (b) Co sites-prior. Insets: the catalytic structure modeling of CoFe-LDH nanozyme (yellow) and L-C-LDH nanozyme (pink).

Application potential of LDH nanozymes

Based on the superior POD-like activities of LDH nanozymes, they exhibit potential application prospects in the field of biosensing. The above mechanism studies have confirmed that LDH nanozymes can decompose H_2O_2 to produce ·OH and $\cdot O_2^-$, and thereby it can be used to determine H_2O_2. Under optimal experimental conditions, various concentrations of H_2O_2 were added to the L-C-LDH/TMB system and Me-L-C-LDH/TMB system, respectively and incubated for 10 min at 37 °C. It can be seen in Fig. S49a and c† that with the increased concentration of H_2O_2, the absorbance at 652 nm was enhanced. Fig. S49b and d† illustrate that when the concentration of H_2O_2 was in the range of 5.00–100 μM, there was a good linear correlation between ΔA, where ΔA = Abs (blank, 652 nm) − Abs (H_2O_2, 652 nm) and the concentration of H_2O_2. The limit of detection (LOD) of H_2O_2 was 0.780 μM and 0.420 μM, respectively. The performances of different reported nanozymes for H_2O_2 detection are illustrated in Table S7† for comparison. Ascorbic acid (AA) can reduce oxTMB and meanwhile, is itself oxidized to dehydroascorbic acid. Based on this property, the L-C-LDH/TMB system and Me-L-C-LDH/TMB system were used to detect the concentration of AA *via* recording the absorbance at 652 nm. As shown in Fig. 7a–c, when the concentration of AA was in the range of 0.050–1.00 μM, there was a good linear correlation between ΔA, where ΔA = Abs (blank, 652 nm) − Abs (AA, 652 nm) and the concentration of AA. The LOD for AA based on the L-C-LDH/TMB system and Me-L-C-LDH/TMB system was 0.024 μM and 0.027 μM, respectively. To demonstrate the selectivity of LDH nanozymes for the detection of AA, some probable interfering substances in practical samples, namely CO_3^{2-}, SO_4^{2-}, SO_3^{2-}, Zn^{2+}, K^+, glycine (Gly), valine (Val), threonine (Thr), glucose (Glu), alanine (Ala), tryptophan (Trp) and leucine (Leu) were added in the reaction system, respectively. As depicted in Fig. S50,† the above usual interfering substances almost had no influence on the absorbance when their concentrations were much higher than that of AA, demonstrating that LDH nanozymes had certain anti-interference selectivity for the detection of AA. The performances of different reported nanozymes for AA determination are illustrated in Table S8† for comparison.

POD-like nanozymes have also been widely used in the antibacterial field. Based on the superior POD-like activities of LDH nanozymes, the antibacterial activities under weak acidic conditions were further studied. *Escherichia coli* (*E. coli*) and *Staphylococcus aureus* (*S. aureus*) were selected as the Gram-negative bacteria model and Gram-positive bacteria model for antibacterial experiments, respectively. As shown in Fig. 7d and e, H_2O_2 at a concentration of 1 mM was almost non-toxic to *E. coli*. However, CoFe-LDH nanozyme, L-C-LDH nanozyme and Me-L-C-LDH nanozyme can kill 35%, 66% and 67% of *E. coli*, respectively, the kill rates of which further increased to 81%, 99% and 99%, respectively in the presence of H_2O_2, that was comparable to that of the reported superb nanozymes.[36,37] To study the bactericidal mechanism of LDH nanozymes, AA was added to the systems, which acted as the inhibitor of ROS. As shown in Fig. S51,† the number of bacterial colonies increased after the addition of AA, indicating that the LDH nanozymes killed bacteria by catalyzing

Open Access Article. Published on 15 March 2024. Downloaded on 6/15/2025 4:25:20 AM.
This article is licensed under a Creative Commons Attribution-NonCommercial 3.0 Unported Licence.

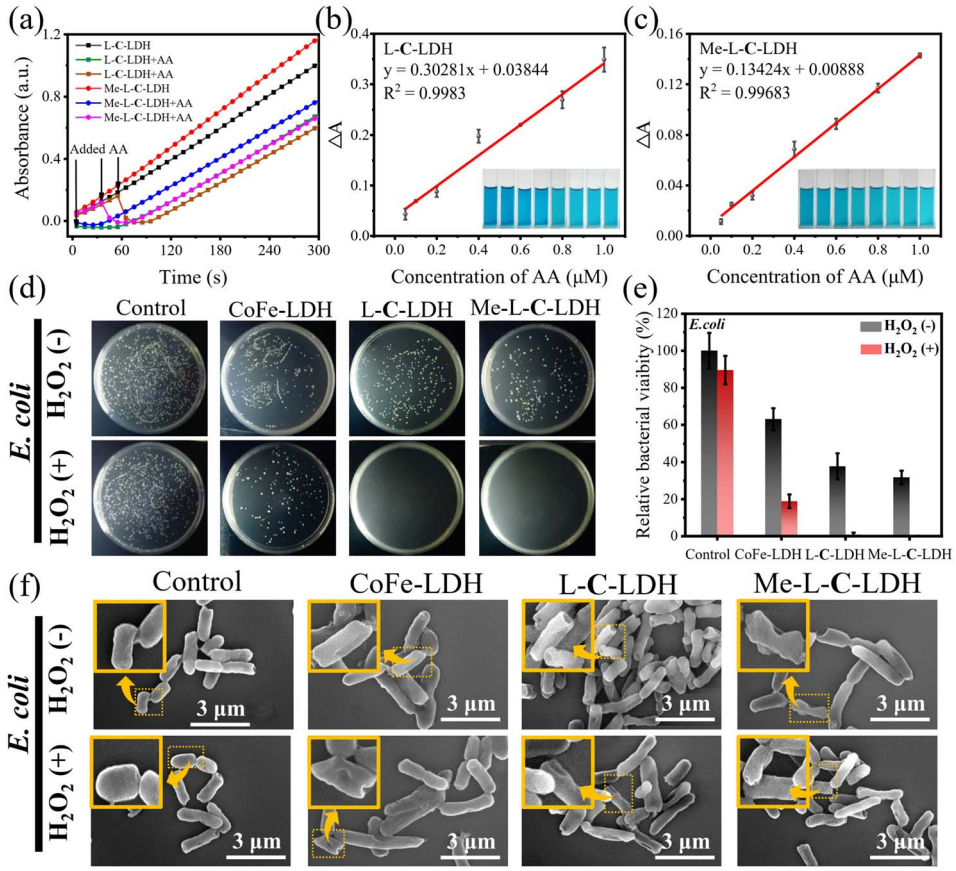

Fig. 7 (a) UV-vis absorption spectra of L-C-LDH nanozyme and Me-L-C-LDH nanozyme with the addition of AA. Relevant dose-responsive linear calibration plot of AA detection based on (b) L-C-LDH nanozyme and (c) Me-L-C-LDH nanozyme. The *in vitro* antibacterial investigation of CoFe-LDH nanozyme, L-C-LDH nanozyme and Me-L-C-LDH nanozyme: (d) the representative culture images of the bacterial colonies and (e) corresponding relative bacterial viability. (f) SEM images of *E. coli* under different treatments (the damaged membranes were indicated with yellow arrows).

the production of ·OH and $\cdot O_2^-$. Furthermore, SEM was used to observe the morphology and membrane integrity of bacteria. As illustrated in Fig. 7f, in the absence of H_2O_2, *E. coli* attached to the surfaces of all samples individually and presented a relatively intact rod-like form, whereas in the presence of H_2O_2, the membranes of *E. coli* underwent partial contraction (yellow arrow) and were damaged. Damaged bacterial membranes would lead to cytoplasmic leakage and disruption of ATP synthesis, thus resulting in bacterial death.[38] In addition, LDH nanozymes also exhibited an antibacterial effect on *S. aureus* (Fig. S52†) and antibiotic resistant bacteria (Fig. S53†). These results indicated that LDH nanozymes exhibited potential broad-spectrum antibacterial activity.

Conclusions

To sum up, a kind of high-efficiency POD mimic has been constructed based on the modulation of the catalytic microenvironment of LDH nanozymes through defect engineering induced by amino acid intercalation. Experimental results and DFT simulations indicated that the intercalation of amino acids can effectively enhance the POD-like activity of LDH nanozymes *via* increasing V_O/V_M of LDH and facilitating electron transport. In particular, L-C-LDH nanozymes exhibited the strongest POD-like activities benefiting from the thiol group. Moreover, amino acid intercalated LDH nanozymes exhibited desirable performance in the detection of H_2O_2 and AA, as well as the elimination of bacteria. Amino acids, which are naturally occurring in nature, are excellent candidates for modifying nanozymes. Regarding the use of amino acids to modify nanozymes, there is still a lot of work worthy of further exploration, such as the comparison of different amino acid derivatives for the regulation of enzyme activity, and whether the unique characteristics and special functional groups of amino acids can provide more new functions to nanozymes. This study provides an original paradigm and a novel idea for engineering high-performance nanozymes.

Data availability

All the data supporting this article have been included in the main text and the ESI.†

Author contributions

Dong Han: synthesis, characterization, data analysis. Kui Yang: data analysis, writing – review & editing. Lanlan Chen:

© 2024 The Author(s). Published by the Royal Society of Chemistry

Open Access Article. Published on 15 March 2024. Downloaded on 6/15/2025 4:25:20 AM. This article is licensed under a Creative Commons Attribution-NonCommercial 3.0 Unported Licence.

characterization, data analysis. Zhaosheng Zhang: data analysis. Chen Wang: synthesis, data analysis. Hongyuan Yan: data analysis, writing – review & editing. Jia Wen: data analysis, writing – review & editing, project administration, supervision.

Conflicts of interest

There are no conflicts to declare.

Acknowledgements

This work was financially supported by the Natural Science Foundation of Hebei Province (No. B2023201031), the Science and Technology Research Project of Hebei Province (QN2023117), the Advanced Talents Incubation Program of Hebei University (No. 521000981345 and No. 521000981343), the Innovation Team Program of Hebei University (IT2023A06) and the Interdisciplinary Project of Hebei University (DXK202310).

Notes and references

1 W. Liu, Y. Zhang, G. Wei, M. Zhang, T. Li, Q. Liu, Z. Zhou, Y. Du and H. Wei, *Angew. Chem., Int. Ed.*, 2023, **62**, e202304465.
2 H. Li, Y. Wen, X. Zhu, J. Wang, L. Zhang and B. Sun, *ACS Sustainable Chem. Eng.*, 2020, **8**, 520–526.
3 C. Peng, Z. Yu, W. Wu, J. Li and E. Wang, *ACS Appl. Mater. Interfaces*, 2023, **15**, 56678–56688.
4 X. Ma, B. Zhang, N. Ma, C. Liu, Y. Miao, X. Liang, S. Guan, D. Li, A. Liu and S. Zhou, *ACS Appl. Mater. Interfaces*, 2023, **15**, 13869–13878.
5 H. Wei, L. Gao, K. Fan, J. Liu, J. He, X. Qu, S. Dong, E. Wang and X. Yan, *Nano Today*, 2021, **40**, 101269.
6 K. Fan, H. Wang, J. Xi, Q. Liu, X. Meng, D. Duan, L. Gao and X. Yan, *Chem. Commun.*, 2017, **53**, 424–427.
7 G. Li, H. Liu, T. Hu, F. Pu, J. Ren and X. Qu, *J. Am. Chem. Soc.*, 2023, **145**, 16835–16842.
8 H. Zhang, G. Li, L. Deng, H. Zeng and Z. Shi, *J. Colloid Interface Sci.*, 2019, **543**, 183–191.
9 R. Ma, J. Liang, K. Takada and T. Sasaki, *J. Am. Chem. Soc.*, 2011, **133**, 613–620.
10 K. Ma, J. P. Cheng, J. Zhang, M. Li, F. Liu and X. Zhang, *Electrochim. Acta*, 2016, **198**, 231–240.
11 F. Chen, X. Wu, R. Bu and F. Yang, *RSC Adv.*, 2017, **7**, 41945–41954.
12 Y. Tang, F. Wu, L. Fang, H. Ruan, J. Hu, X. Zeng, S. Zhang, H. Luo and M. Zhou, *Prog. Org. Coat.*, 2023, **174**, 107299.
13 T. Hu, L. Yan, Z. Wang, W. Shen, R. Liang, D. Yan and M. Wei, *Chem. Sci.*, 2021, **12**, 2594–2603.
14 M. Wei, J. Guo, Z. Shi, Q. Yuan, M. Pu, G. Rao and X. Duan, *J. Mater. Sci.*, 2007, **42**, 2684–2689.
15 P. Wang, L. Yin, X. Wang, G. Zhao, S. Yu, G. Song, J. Xie, A. Alsaedi, T. Hayat and X. Wang, *J. Environ. Manage.*, 2018, **217**, 468–477.
16 X. Shen, H. Li, Y. Zhang, T. Ma, Q. Li, Q. Jiao, Y. Zhao, H. Li and C. Feng, *Appl. Catal., B*, 2022, **319**, 121917.
17 C. Hao, Y. Wu, Y. An, B. Cui, J. Lin, X. Li, D. Wang, M. Jiang, Z. Cheng and S. Hu, *Mater. Today Energy*, 2019, **12**, 453–462.
18 S. Nagappan, A. Karmakar, R. Madhu, S. S. Selvasundarasekar, S. Kumaravel, K. Bera, H. N. Dhandapani, D. Sarkar, S. M. Yusuf and S. Kundu, *ACS Appl. Energy Mater.*, 2022, **5**, 11483–11497.
19 Z. Song, Y. Xu, H. Wu, J. Huang and Y. Zhang, *J. Environ. Manage.*, 2023, **344**, 118523.
20 S. Ma, L. Huang, L. Ma, Y. Shim, S. M. Islam, P. Wang, L.-D. Zhao, S. Wang, G. Sun, X. Yang and M. G. Kanatzidis, *J. Am. Chem. Soc.*, 2015, **137**, 3670–3677.
21 Y. S. Yun, V.-D. Le, H. Kim, S.-J. Chang, S. J. Baek, S. Park, B. H. Kim, Y.-H. Kim, K. Kang and H.-J. Jin, *J. Power Sources*, 2014, **262**, 79–85.
22 X. Wang, L. Qin, M. Lin, H. Xing and H. Wei, *Anal. Chem.*, 2019, **91**, 10648–10656.
23 Y. He, M. Feng, X. Zhang and Y. Huang, *Anal. Chim. Acta*, 2023, **1283**, 341959.
24 L. Wu, Z. Sun, Y. Zhen, S. Zhu, C. Yang, J. Lu, Y. Tian, D. Zhong and J. Ma, *Environ. Sci. Technol.*, 2021, **55**, 15400–15411.
25 S. Wang, J. Zhu, T. Li, F. Ge, Z. Zhang, R. Zhu, H. Xie and Y. Xu, *Environ. Sci. Technol.*, 2022, **56**, 7924–7934.
26 L. Wu, J. Hong, Q. Zhang, B.-Y. Chen, J. Wang and Z. Dong, *Chem. Eng. J.*, 2020, **385**, 123620.
27 Y. Ning, Y. Sun, X. Yang, Y. Li, A. Han, B. Wang and J. Liu, *ACS Appl. Mater. Interfaces*, 2023, **15**, 26263–26272.
28 X. Cheng, Y. Xie, G. Li, Z. Zheng and Q. Kuang, *Inorg. Chem. Front.*, 2023, **10**, 2335–2343.
29 W. Shen, T. Hu, X. Liu, J. Zha, F. Meng, Z. Wu, Z. Cui, Y. Yang, H. Li, Q. Zhang, L. Gu, R. Liang and C. Tan, *Nat. Commun.*, 2022, **13**, 3384.
30 R. Liu, Y. Wang, D. Liu, Y. Zou and S. Wang, *Adv. Mater.*, 2017, **29**, 1701546.
31 D. Chen, Z. Xia, Z. Guo, W. Gou, J. Zhao, X. Zhou, X. Tan, W. Li, S. Zhao, Z. Tian and Y. Qu, *Nat. Commun.*, 2023, **14**, 7127.
32 X. Wei, S. Song, W. Song, Y. Wen, W. Xu, Y. Chen, Z. Wu, Y. Qin, L. Jiao, Y. Wu, M. Sha, J. Huang, X. Cai, L. Zheng, L. Hu, W. Gu, M. Eguchi, T. Asahi, Y. Yamauchi and C. Zhu, *Chem. Sci.*, 2022, **13**, 13574–13581.
33 D. Yu, J. He, Z. Wang, H. Pang, L. Li, Y. Zheng, Y. Chen and J. Zhang, *Chem. Eng. J.*, 2021, **417**, 129240.
34 L. Wang, Z. Yang, G. Song, Z. You, X. Zhang, L. Liu, J. Zhang, L. Ding, N. Ren, A. Wang, J. Liu, H. Liu and X. Yu, *Appl. Catal., B*, 2023, **325**, 122345.
35 B. Wang, Y. Fang, X. Han, R. Jiang, L. Zhao, X. Yang, J. Jin, A. Han and J. Liu, *Angew. Chem., Int. Ed.*, 2023, **62**, e202307133.
36 M. N. Karim, M. Singh, P. Weerathunge, P. Bian, R. Zheng, C. Dekiwadia, T. Ahmed, S. Walia, E. D. Gaspera, S. Singh, R. Ramanathan and V. Bansal, *ACS Appl. Nano Mater.*, 2018, **1**, 1694–1704.
37 D. Mehta, P. Sharma and S. Singh, *Colloids Surf., B*, 2023, **231**, 113531.
38 D. Zhang, R. Xu, S. Chen, H. Du, S. Qian, F. Peng and X. Liu, *Bioact. Mater.*, 2023, **30**, 15–28.